# Dynamic Glucose-Enhanced (DGE) MRI: Translation to Human Scanning and First Results in Glioma Patients

**Xiang Xu[1,5], Nirbhay N. Yadav[1,5], Linda Knutsson[7], Jun Hua[1,5], Rita Kalyani[2], Erica Hall[2], John Laterra[3,6], Jaishri Blakeley[3,6], Roy Strowd[3,6], Martin Pomper[1], Peter Barker[1,5], Kannie W. Y. Chan[1,5], Guanshu Liu[1,5], Michael T. McMahon[1,5], Robert D. Stevens[1,3,4,5], and Peter C.M. van Zijl[1,5]**

[1]Russell H. Morgan Department of Radiology and Radiological Science, [2]Division of Endocrinology, Diabetes and Metabolism, and [3]Departments of Neurology, Oncology, and Neuroscience and [4]Anesthesiology and Critical Care Medicine, Johns Hopkins University School of Medicine, Baltimore, MD; [5]F.M. Kirby Research Center for Functional Brain Imaging and [6]Hugo W. Moser Research Institute, Kennedy Krieger Institute, Baltimore, MD; and [7]Department of Medical Radiation Physics, Lund University, Lund, Sweden

**Corresponding Author:**
Peter C.M. van Zijl, PhD
F.M. Kirby Research Center, Kennedy Krieger Research Institute, 707 N. Broadway, Baltimore, MD 21205;
E-mail: pvanzijl@mri.jhu.edu

**Key Words:** D-glucose, perfusion, chemical exchange saturation transfer, CEST, dynamic glucose-enhanced MRI, glioma patients

**Abbreviations:** Anaplastic astrocytoma (AA), area under the curve (AUC), arterial input function (AIF), blood-brain barrier (BBB), cerebral blood flow (CBF), cerebral blood volume (CBV), chemical exchange saturation transfer (CEST), cerebral spinal fluid (CSF), dynamic contrast enhanced (DCE), dynamic glucose enhanced (DGE), dynamic susceptibility contrast (DSC), echo time (TE), extravascular extracellular space (EES), flip angle (FA), Food and Drug Administration (FDA), Gadolinium (Gd), gadolinium-based contrast agent (GBCA), chemical exchange saturation transfer measurement sensitized to the presence of glucose (glucoCEST), glioblastoma multiforme (GBM), magnetic resonance imaging (MRI), region of interest (ROI), signal to noise ratio (SNR), repetition time (TR), World Health Organization (WHO)

ABSTRACT

Recent animal studies have shown that D-glucose is a potential biodegradable magnetic resonance imaging (MRI) contrast agent for imaging glucose uptake in tumors. We show herein the first translation of that use of D-glucose to human studies. Chemical exchange saturation transfer (CEST) MRI at a single frequency offset optimized for detecting hydroxyl protons in D-glucose was used to image dynamic signal changes in the human brain at 7 T during and after D-glucose infusion. Dynamic glucose enhanced (DGE) image data from 4 normal volunteers and 3 glioma patients showed a strong signal enhancement in blood vessels, while a spatially varying enhancement was found in tumors. Areas of enhancement differed spatially between DGE and conventional gadolinium-enhanced imaging, suggesting complementary image information content for these 2 types of agents. In addition, different tumor areas enhanced with D-glucose at different times after infusion, suggesting a sensitivity to perfusion-related properties such as substrate delivery and blood-brain barrier (BBB) permeability. These preliminary results suggest that DGE MRI is feasible for studying glucose uptake in humans, providing a time-dependent set of data that contains information regarding arterial input function, tissue perfusion, glucose transport across the BBB and cell membrane, and glucose metabolism.

## INTRODUCTION

Current clinical practice for detecting malignant brain tumors by magnetic resonance imaging (MRI) is based on the use of gadolinium-based contrast agents (GBCAs) to enhance regions with blood-brain barrier (BBB) disruption. Although used on a daily basis, this modality still faces many challenges. For example, roughly 10% of glioblastoma multiformes (GBMs) and 30% of anaplastic astrocytomas (AAs) demonstrate no enhancement (1, 2). Gadolinium enhancement itself cannot distinguish between different causes of BBB disruption and will visualize both tumor regrowth (progression) and the effects of treatment (pseudoprogression) (3, 4). Although more advanced dynamic contrast enhanced (DCE) approaches show potential for such differentiation (5), these methods are not yet standard in the clinic. In addition to those diagnostic and prognostic limitations, the safety of GBCAs has been challenged. People with moderate to advanced kidney failure who receive gadolinium are at risk of developing nephrogenic systemic fibrosis/nephrogenic fibrosing dermopathy (6). GBCAs have now been labeled with a warning for nephrogenic systemic fibrosis, and patients need to be screened for renal dysfunction. In addition, GBCAs are currently under investigation by the Food and Drug Administration (FDA) because they may be retained in the deep gray matter nuclei for longer periods of time (7, 8). Based on such issues with the standard agent, there is an urgent


ISSN 2379-1381 http://dx.doi.org/10.18383/j.tom.2015.00175

**Table 1.** Patient Characteristics

| Participant Number | Sex | Decade of Birth | Initial Histopathologic Diagnosis | Therapy Prior to DGE | Diagnosis at Time of DGE |
|---|---|---|---|---|---|
| 1 | Male | 1990 | Anaplastic astrocytoma (WHO grade III)[a] | None | Anaplastic astrocytoma |
| 2 | Male | 1960 | Glioblastoma (WHO grade IV) | Surgery, radiation, temozolomide, experimental agent | Glioblastoma |
| 3 | Female | 1980 | Low-grade astrocytoma (WHO grade II) | Surgery, radiation | Glioblastoma |

WHO indicates World Health Organization.
[a] DGE scan performed before initial histopathologic diagnosis.

need for developing novel (preferably nonsynthetic) agents that are associated with minimal risk.

To our knowledge, all MRI contrast agents used currently in the clinic have been synthetic, with most based on paramagnetic metal complexes. The potential toxicity of such compounds depends on the thermodynamic and kinetic stability of coordination. Our goal is to develop nonmetallic biocompatible contrast agents for clinical MRI. Recent experiments in animal tumor models have shown that D-glucose has potential as a biodegradable contrast agent that can be detected using the chemical exchange saturation transfer (CEST) technique (glucoCEST) (9-12) or relaxation-based ($T_1\rho$ or $T_2$) approaches (13-16). Glucose derivatives detectable by CEST have also been suggested (10, 11, 17). More recently, the use of dynamic glucose enhanced (DGE) imaging was demonstrated in a animal model with human glioma xenografts (18), allowing increased BBB permeability to be visualized in tumors. The systemic administration of natural D-glucose (from corn, also known as dextrose) in humans has been routinely used in intravenous glucose-tolerance testing (19), allowing us to translate this approach to human imaging studies rapidly and safely. Herein, we provide a first demonstration of the feasibility of DGE-MRI in 4 normal volunteers and in 3 patients with glioma.

## METHODS

### Protocol

All studies were approved by the Institutional Review Board at the Johns Hopkins University School of Medicine, and informed consent was obtained before the study from all participants. For these first studies, limited to age group 18 - 75 years, all participants were required to fast for at least 8 hours and have a baseline fasting glucose level within the normal range of 70 mg/dL (3.9 mM) to 125 mg/dL (7 mM), as based on the standards of care in diabetes (20). Furthermore, in addition to typical MRI- and gadolinium-based exclusion criteria, we used the following conservative glucose-related exclusion criteria for recruitment: persons with diabetes mellitus (self-reported or hemoglobin A1c $\geq$6.5%), sickle cell disease, or blood iron deficiency (hemoglobin concentration $<$12 g/dL or hematocrit $<$35%). We had additional exclusion criteria for patients, namely hypertension (high blood pressure) requiring medication, multiple myeloma, solid organ transplant, or history of severe hepatic disease/liver transplant/pending liver transplant. For healthy volunteers, additional exclusion criteria were seizure disorder and prescription medicine intake.

After checking the baseline glucose level to be within the normal range specified above, a brief hyperglycemic state was instituted by intravenous infusion of hospital-grade D50 glucose (50% dextrose or 25 g of dextrose in a 50-mL sterile water solution; Hospira, Lake Forest, IL) in 1 arm. Because this was done manually, the infusion length varied, generally from 1 to 1.2 min. The venous glucose level was monitored periodically by sampling the blood from a vein in the contralateral arm before and at set times after glucose infusion and measuring glucose concentration using a blood analyzer (Radiometer, Copenhagen, Denmark). The range of glucose levels after glucose infusion found in volunteers inside and outside (early protocol testing) the magnet ranged from a minimum of 10.5 mM (189 mg/dL) to a maximum of 23.7 mM (427 mg/dL), with a median of 15.4 mM (277 mg/dL). The time of peak varied but generally occurred within 2-4 min after infusion. These levels did not correlate with the weight of the participant, indicating that weight may not be a good indicator of the glucose response curve, which is more likely determined by the participant's insulin response.

### Subjects

The study was conducted on 4 healthy volunteers and 3 participants with malignant gliomas (Table 1). The 3 participants (2 men, 1 woman) had a median age of 33 years (range, 22-46). Participant 1 was found to have a right insular nonenhancing lesion after presenting with seizure and underwent DGE before his first procedure. The final diagnosis was AA. Participant 2 had a known left-frontal GBM status after standard chemoradiation and an experimental agent completed 7 months before DGE imaging. Repeat resection after DGE imaging confirmed recurrent GBM. Participant 3 had a biopsy-confirmed low-grade astrocytoma treated with radiation therapy 7 years before presenting with radiographic progression of a left-frontal lesion. DGE imaging was performed prior to resection that revealed GBM.

### Data Acquisition

Subjects were scanned on a 7 T Philips MRI scanner (Philips Healthcare, Best, The Netherlands). A 32-channel phased-array head coil (Nova Medical, Wilmington, MA) was used for radiofrequency reception and a head-only quadrature coil for transmission. The saturation was achieved using a train of 32 sinc-gauss pulses, B1 = 1.96 $\mu$T, with each pulse 50 ms long and separated by a 25 ms delay. The images were acquired using a

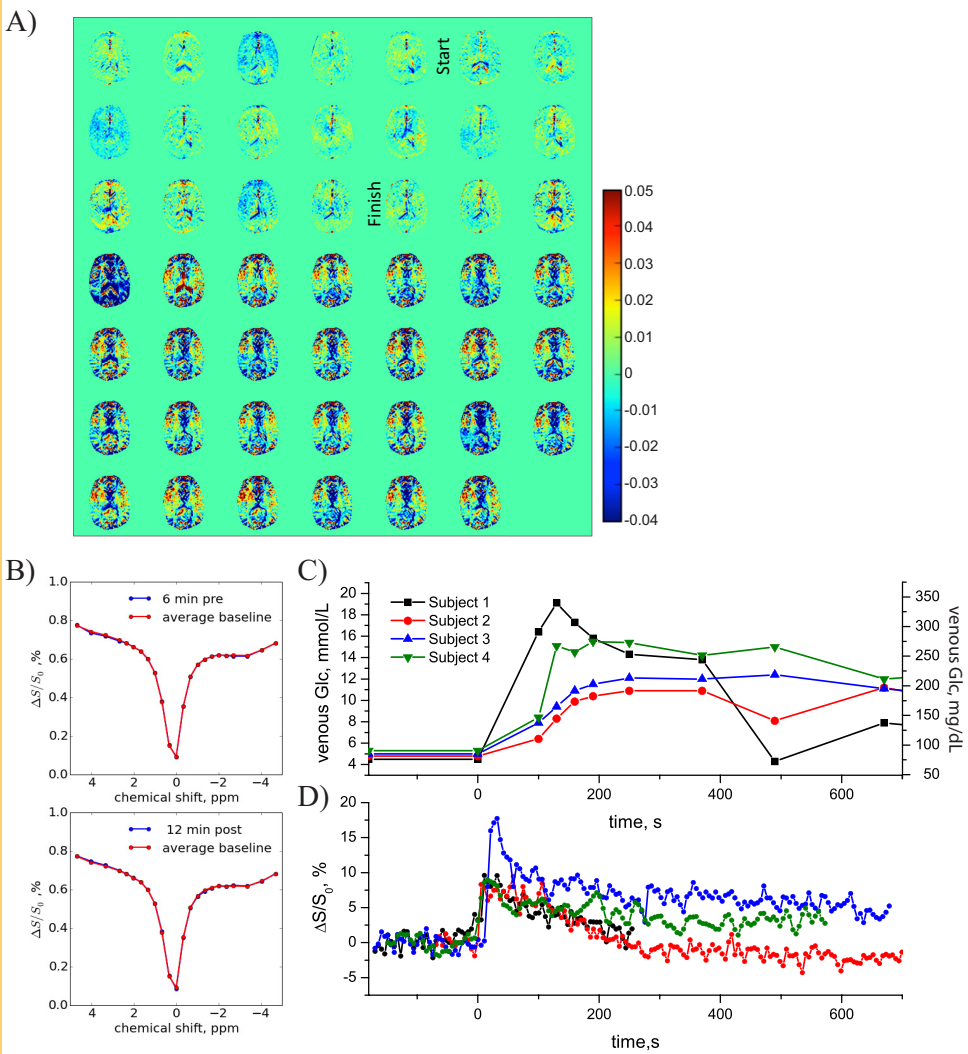


**Figure 1.** Healthy volunteer. (A) DGE difference images (5.3-s time resolution). (B) *z*-spectra in ventricle (blue) before (top) and after infusion (bottom) compared to average baseline (red). No difference is visible. (C) Venous blood glucose concentrations measured in 4 volunteers. (D) DGE signal evolution in an arterial vessel for these volunteers.

single-shot turbo gradient echo with TR (between each echo)/TE/FA = 5 ms/1.48 ms/30°. The SENSE acceleration factor was 2 (Anterior-Posterior). A single 6 mm thick slice across a field of view of 224 × 224 mm$^2$ with 3 × 3 mm$^2$ in-plane resolution was acquired. A 2 s delay was introduced after each dynamic scan to recover longitudinal magnetization; therefore, the dynamic images were acquired at a temporal resolution of 5.3 s. Saturation spectra as a function of frequency in the proton spectrum (the so-called *z*-spectra) were acquired before and after the dynamic scan. For DGE-MRI, the acquisition of a full *z*-spectrum is not necessary, and data were acquired at a saturation offset frequency of 1.2 ppm, where 3 of the hydroxyl protons of glucose resonate (21, 22). Two protocols were used for the dynamic scan. For 1 of the healthy volunteers and the first participant with glioma, 70 dynamics were acquired with a total scan time of 6 min 17 s. Because the glucose level remained high for longer than this period, we increased that to at least 160 dynamics or a total scan time of ≥14.5 min for other volunteers and participants with glioma. The glucose infusion started at time point 90 s (for short protocol) or 180 s (for longer protocols) into the dynamic scan, and the infusion time ranged from 62 to 72 s.

## Data Analysis

For datasets with extensive motion, the images were registered to the third image in the dynamic series using the rigid-body (6 degrees of freedom) registration algorithm FLIRT (FSL; FMRIB Center, University of Oxford, Oxford, UK) with the normalized mutual information cost function and sinc resampling. However, the motion correction approach was limited because of the use of single-slice acquisition.

For the DGE data, the first 2 images were discarded to assure proper steady state, and the image intensities ($S$) of the others were normalized by dividing with the pre-infusion $S_0$ image. Baseline images with intensity $S_{\text{base}}$ were generated by averaging all of the pre-infusion images. Glucose dynamic difference images were generated by taking the difference between each dynamic image intensity $S(t_n)$ and $S_{\text{base}}$. The dynamic curves for the regions of interest (ROIs) of the healthy volunteer and participants 2 and 3 were smoothed using a 3-point moving average. The DGE area under the curve (AUC) was calculated using

$$\text{AUC} = \sum_1^n \frac{S_{base}}{S_0} - \frac{S(t_n)}{S_0} = \sum_1^n \frac{\Delta S(t_n)}{S_0},$$

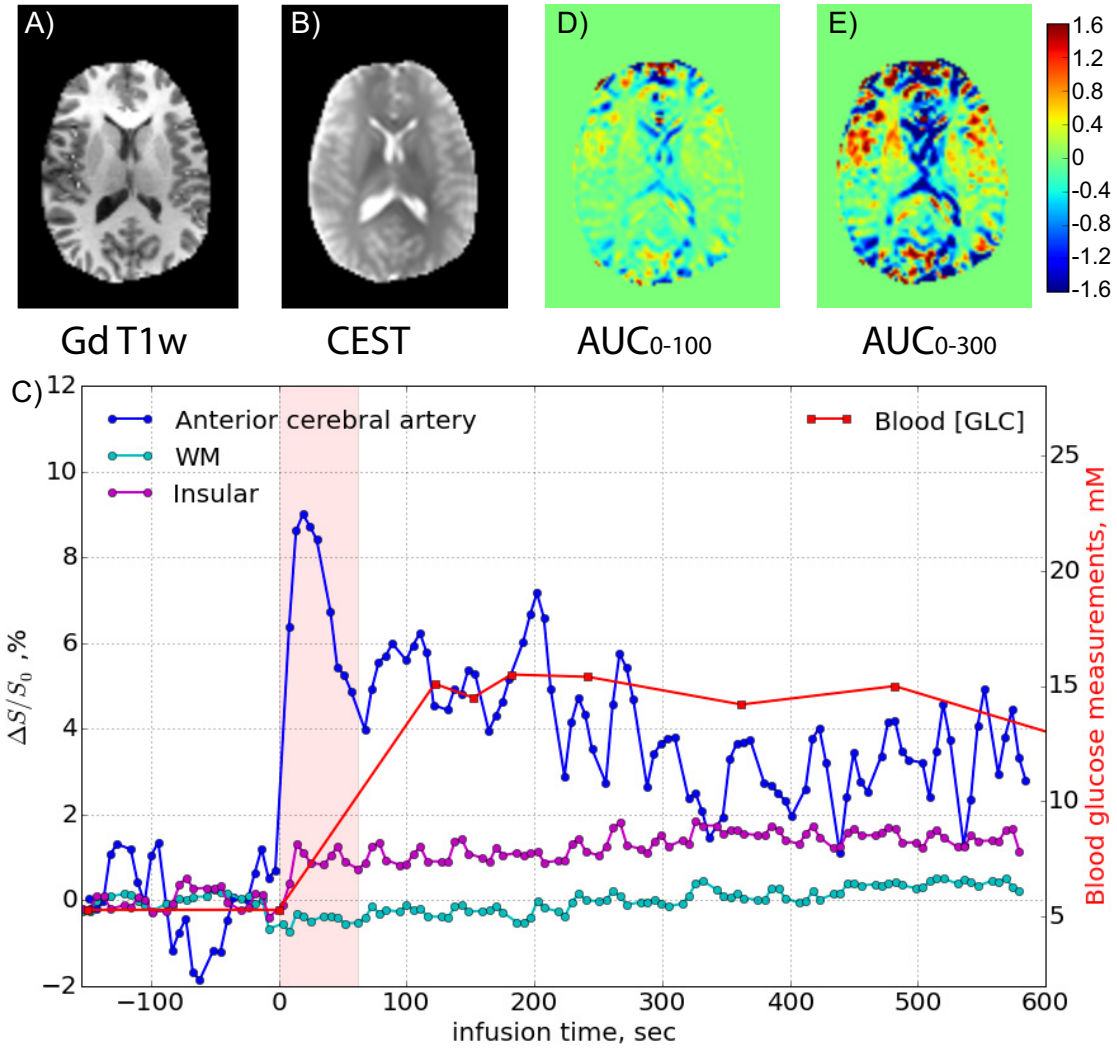


**Figure 2.** (A) Gadolinium-$T_1$-weighted image acquired 1 h after DGE, (B) CEST raw image with ROIs, and (D, E) DGE-based AUC images for 2 different time periods relative to the start of infusion for the volunteer shown in Figure 1A. The time curves for several regions of interest are shown in (C).

in which $n$ can be chosen based on the information of the DGE image evolution after glucose infusion.

## RESULTS

### Healthy Volunteers

Figure 1A shows an example of dynamic glucose-enhanced difference images with signal difference intensity $\Delta S(t)/S_0 = [S_{base} - S(t)]/S_0$, obtained upon infusing glucose in a volunteer, with the start and finish of the infusion indicated. Notice that the signal is subtracted from the average baseline so that a positive intensity in these images reflects more saturation transfer (water-intensity loss in the MRI) because of an increased concentration in glucose in an image voxel. The DGE pattern seen was typical for all volunteers, namely first an increase in vascular signal intensity and later a slight increase in glucoCEST signal in tissue. Interestingly, a DGE signal reduction (blue contrast) is visible around cerebral spinal fluid (CSF)-rich spaces such as the ventricles and cortex. An increase of glucose concentration in the CSF is expected to increase saturation slightly at the frequency of 1.2 ppm, so the result of reduced saturation at first seems puzzling. We investigated this effect by studying the saturation profiles ($z$-spectra) acquired before and after infusion for an ROI chosen well within the ventricles, which showed a negligible change in width for CSF (Figure 1B). However, it is known that glucose is readily taken up into the CSF and can cause volumetric changes at the concentrations used for our studies (23). A tentative explanation for the saturation loss is that because of the volume increase and the partial volume effects between the narrow $z$-spectrum of CSF and the broad $z$-spectrum of tissue, some voxels around CSF spaces will appear hypointense as a result of an overall narrowing of the signal.

Figure 1C shows the time dependence of the measured venous blood glucose concentration in the contralateral arm of 4 normal volunteers. Figure 1D shows the corresponding in-

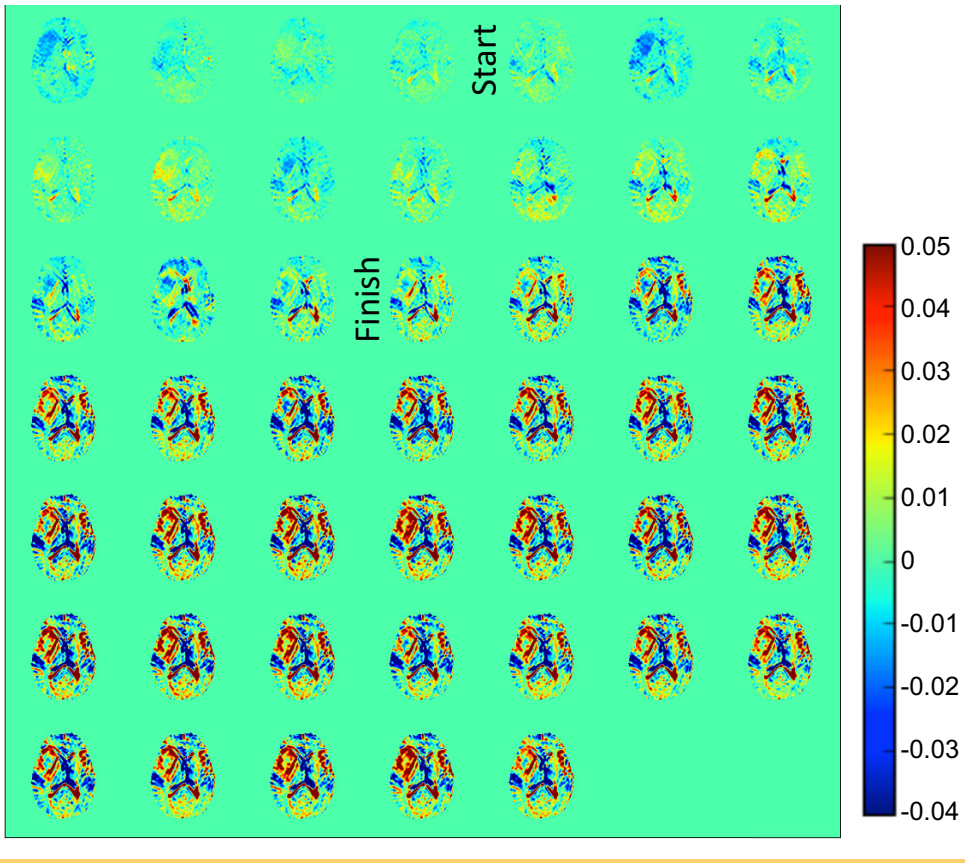


**Figure 3.** DGE difference images (5.3-s time resolution) for participant 1 with anaplastic astrocytoma. A video of this wash-in process is available in the online version of this article (PLAY VIDEO).

creases in water saturation fraction as measured in a single voxel in a sufficiently large arterial vessel (eg, the anterior cerebral artery) visible in the image. An 8-18% saturation increase that resulted from the effect of glucose infusion was consistently detected in the arterial blood of the volunteers, showing that it should in principle be possible to obtain an arterial input function (AIF) with dynamic glucoCEST. That will require a calibration to relate the water saturation increase in blood to absolute glucose concentration. Notice that the time scales of the actual blood sampling and the AIF are very different and that the blood sampling does not catch the initial part of the saturation curve. There is correspondence at the later time points, but the actual blood sampling and AIF are not easy to compare because the AIF signal intensities very much depend upon the chosen voxel in the artery, which is generally affected by partial volume effects with surrounding tissue. Future improvements in spatial resolution may resolve this issue, which is well known from the DCE and DSC literature.

Figure 2, panels A and B, show gadolinium-enhanced and CEST anatomical reference images, respectively. Figure 2C shows the dynamic response curves of several ROIs (anterior cerebral artery, white matter, and an insular vessel) together with the blood glucose concentration. The blood sampling started after the initial maximum in the AIF, but after that, the tissue and vessel intensities follow the AIF and blood level quite well. AUC images over different time periods after the start of infusion were calculated and are shown in Figure 2, panels D and E. These images mainly highlight the vessels and show a reduction in CSF spaces that can be used as a reference for the images obtained in the setting of malignant glioma.

## Participants With Glioma

Figure 3 shows DGE difference images for participant 1 with a right hemispheric non-gadolinium-enhancing infiltrative mass as observed on a clinical MRI with gadolinium scan for surgical planning performed a few hours after the DGE study. This participant was ultimately diagnosed as having an AA. On the DGE images, it can again be seen that vessel-rich areas enhance rapidly, whereas some regions around CSF spaces exhibit reduced saturation. Figure 4, panels A and B, show $T_2$-weighted and postgadolinium contrast $T_1$-weighted images, respectively, for this participant, performed at 3 T before surgery. Interestingly, the DGE-MRI areas that show hyperintensity (Figure 3, red) directly after finishing the glucose infusion seem to match the $T_2$-weighted MRI in areas of contralateral vasculature (red arrow) and in a hyperintense rim at the medial outer edge of the tumor (yellow arrow).

The dynamic response curves of several ROIs (anterior cerebral artery, tumor core, lateral tumor rim, and contralateral vessel area) are shown in Figure 4C. The venous glucose concentration measured independently with the glucose analyzer is also plotted and compared in a manner scaled with the AIF, showing similar temporal changes. The signal in the lateral tumor rim ultimately changed by approximately 5% after glucose infusion, but this increase was delayed by at least 100 s. As a first approach in relating the dynamic glucose images to tissue perfusion-related properties, AUC images over different time periods after the start of the infusion were calculated and are shown in Figure 4, panels D–F. No contrast is visible in the tumor core, most likely indicating poor tissue perfusion. It can be seen that the D-glucose slowly infiltrates the tumor rim in a

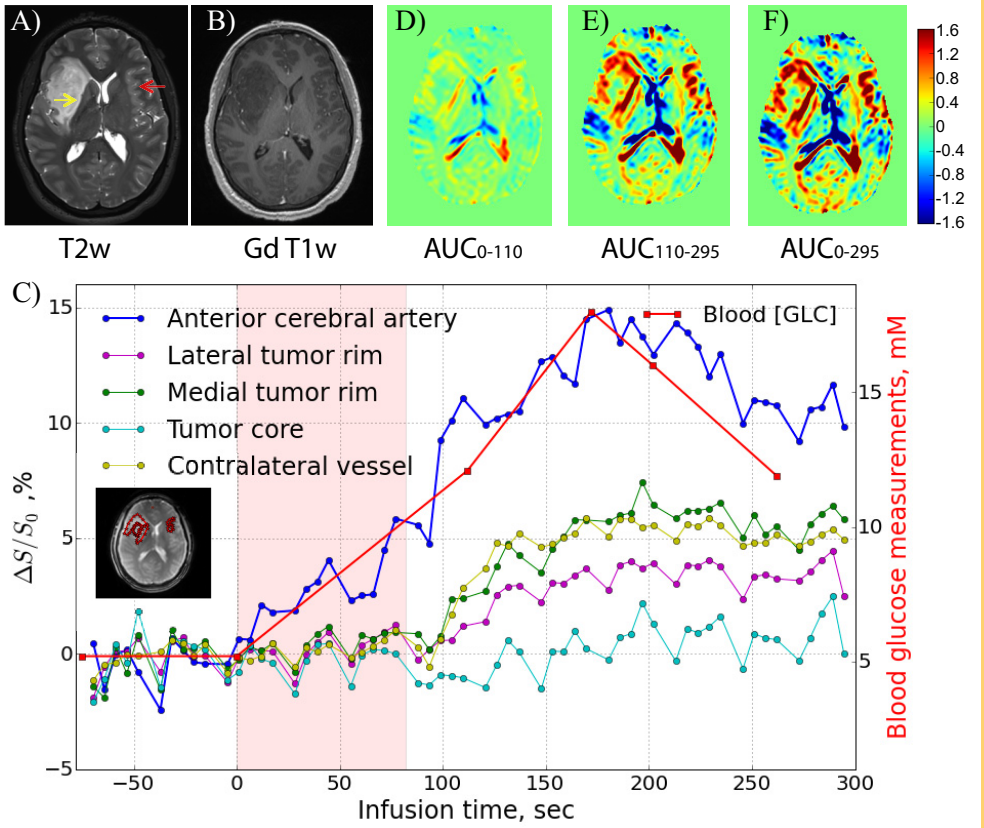


**Figure 4.** Post-DGE and presurgical (A) $T_2$-weighted, (B) gadolinium-$T_1$-weighted, and (D–F) DGE-based AUC images for different time periods relative to the start of infusion for the participant shown in Figure 3. The dynamic time curves for several regions of interest are shown in (C).

time-dependent manner that seems very similar to the AIF. The fact that the DGE scan showed enhanced uptake whereas the postgadolinium $T_1$-weighted image did not is interesting in light of the ultimate diagnosis of AA and may indicate that the small glucose molecule (0.180 kDa) is more sensitive to subtle dysfunction of the BBB associated with more aggressive gliomas than larger molecules such as gadolinium diethylene triamine pentaacetic acid (0.546 kDa) or its analogs. Note that glucose can be transported into the brain in a facilitated manner by glucose transporters but that alterations in BBB permeability may increase the rate of transport through improved diffusivity mechanisms.

Figure 5 shows DGE difference maps recorded for participant 2 with a recurrent left-frontal GBM. Again, the blood vessels are enhanced first, and CSF-rich areas show reduced saturation. Clinical $T_1$-weighted gadolinium images (Figure 6A) show 2 areas of enhancement, namely a rim around a previous surgical cavity and a distinct second region in the middle of the tumor (dubbed lesion 2) as judged from the signal reduction in the $T_1$-weighted MRI. The dynamic time curves for 3 tumor regions of interest (Figure 6B) and contralateral white matter are displayed in Figure 6C, together with the blood glucose level measured in the contralateral arm. Despite the fact that the blood glucose reached only 12 mM, we could still detect DGE changes. Unfortunately, there was brain motion over a period of about 50 s (starting at about 80 s), which is reflected in large intensity variations. This prohibited us from acquiring a proper AIF, which typically is taken from 1 or 2 voxels. Figure 6, D–F, show AUC images acquired over different time periods after the onset of infusion, again indicating a different speed of uptake for different tumor regions. Despite the motion, it is clear that the rim around the necrotic region enhanced rapidly (Figure 6C, dark blue curve), whereas the tumor center and lesion 2 enhanced more slowly.

Figure 7 shows the DGE difference images for participant 3, who had previously undergone needle biopsy and radiotherapies for a left-hemispheric, low-grade astrocytoma. The clinical gadolinium-$T_1$-weighted images show strong enhancement in a rim region lateral to the previous surgical cavity as well as in a circular region (lesion 2) medial to the bottom half of that cavity (Figure 8A). The CEST image (Figure 8B) confirms the presence of a lesion. This participant moved during the scan, so the DGE data were not of the same quality as for the other participants. When taking ROIs (Figure 8B) in the rim, necrotic center, lesion 2 (corresponding to the large bright area in Figure 8A), and contralateral white matter, the motion is well reflected in the corresponding time curves in Figure 8C. However, despite the motion and the fact that the blood glucose concentration never exceeded 11 mM (Figure 8C), the data were still useful because we could construct AUC images over the periods 0-5 and 5-10 min after infusion, showing lesional enhancement first in an area corresponding to the bright lateral rim in the gadolinium-weighted MRI and subsequently more in the lesion core.

## DISCUSSION

To our knowledge, these data demonstrate for the first time the feasibility of acquiring DGE images in humans and of constructing time-selective AUC curves based on certain periods after infusing the D-glucose bolus, which highlight biologically distinct areas of the tumor. The potential of this information to

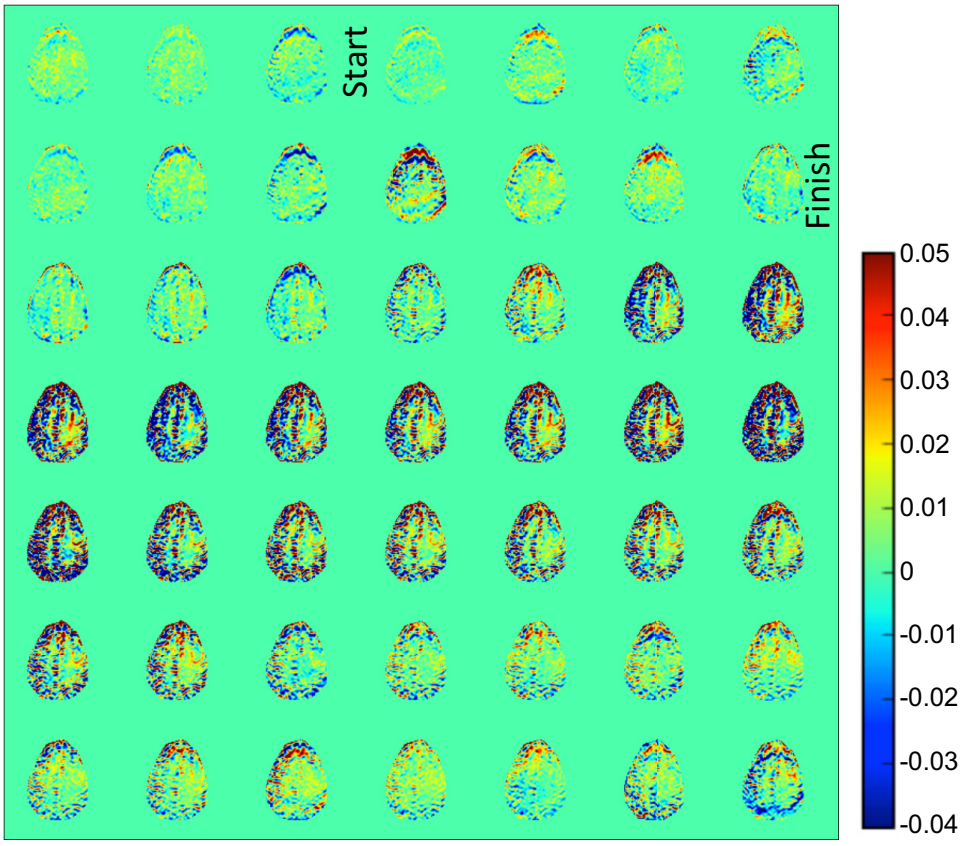


**Figure 5.** DGE difference images (5.3-s time resolution) for participant 2 with a recurrent glioblastoma.

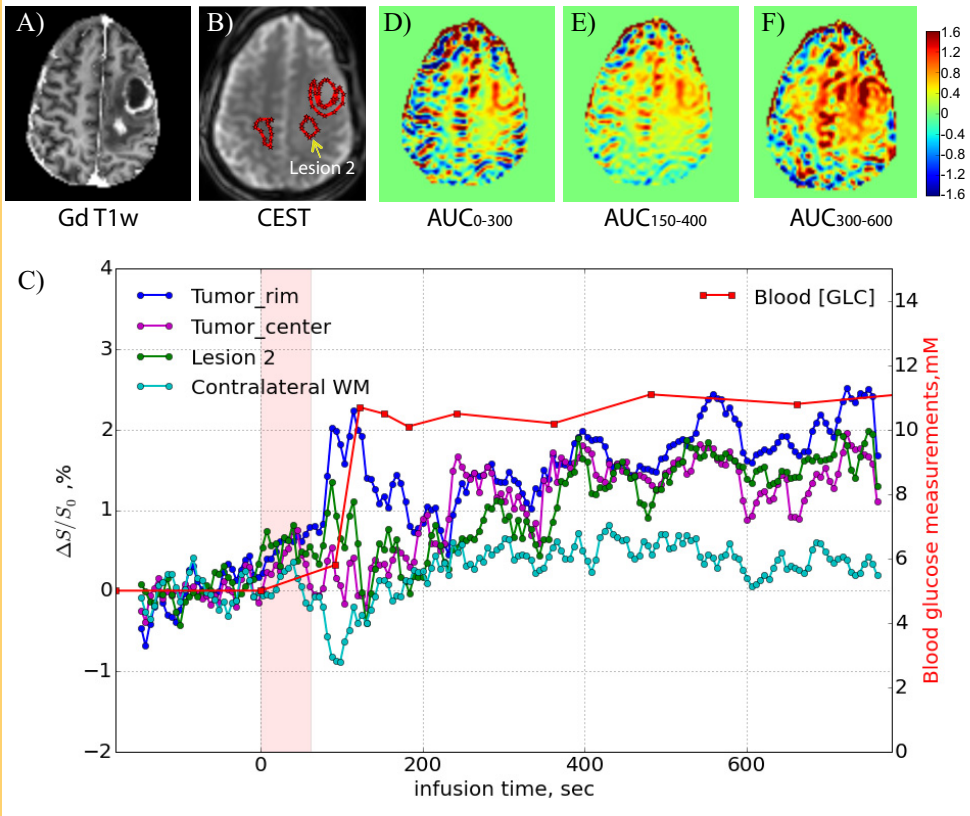


**Figure 6.** (A) Post-DGE and pre-surgical gadolinium $T_1$-weighted image, (B) CEST raw image with ROIs, and (D–F) DGE-based AUC images for different time periods relative to the start of infusion for the participant shown in Figure 5. The time curves for several ROIs are shown in (C). Notice the motion artifacts from 60 to 130 s.

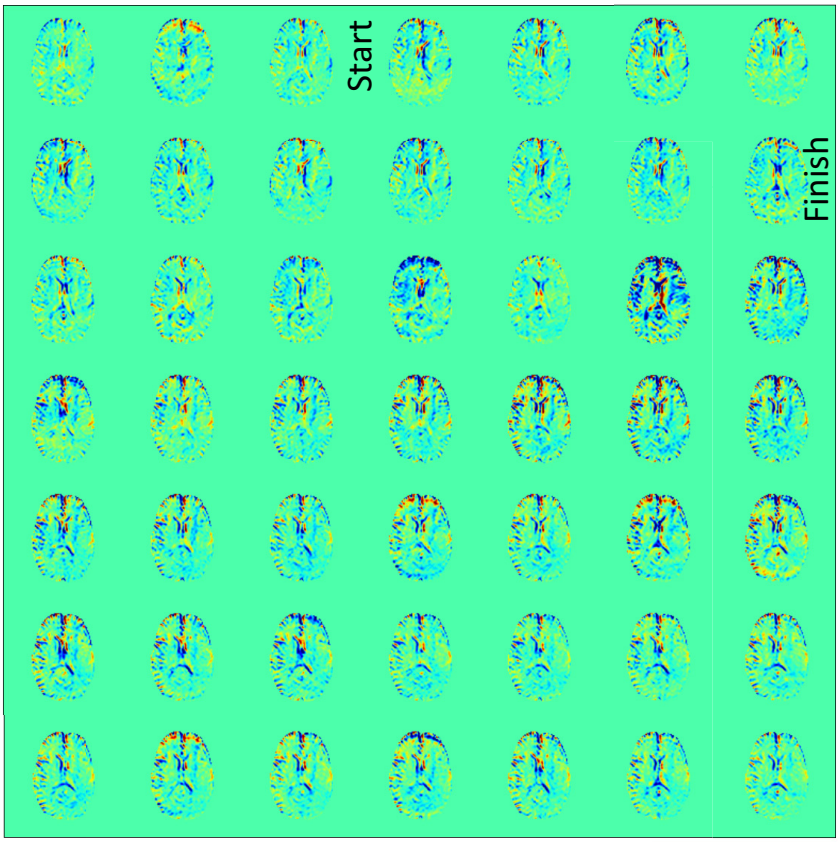


**Figure 7.** DGE difference images (5.3 s time resolution) for participant 3, who was initially operated for a low-grade glioma that subsequently progressed to glioblastoma.

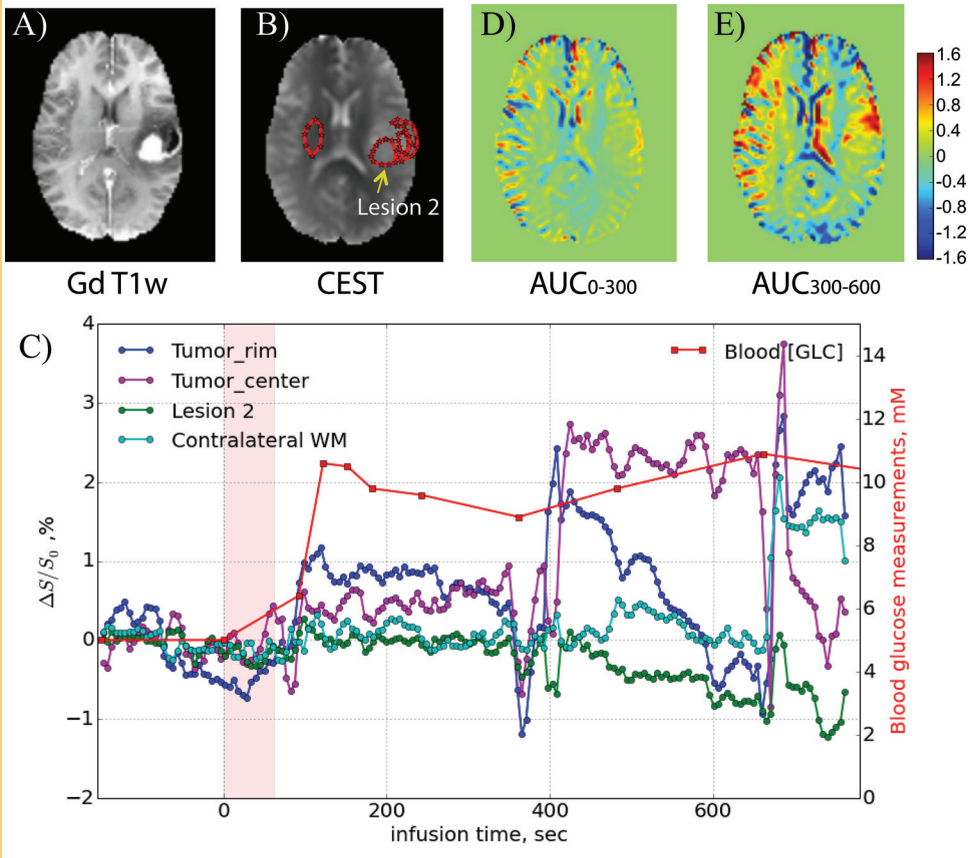


**Figure 8.** (A) Post-DGE and presurgical gadolinium-$T_1$-weighted image, (B) CEST raw image with ROIs, and (D, E) DGE-based AUC images for different time periods relative to the start of infusion for the participant shown in Figure 7. The time curves for several ROIs are shown in (C), showing the effects of movement during several periods.

serve as a sensitive substitute for traditional contrast agents to reveal subtle differences in BBB permeability for different tumor regions will have to be evaluated in future studies on larger groups of patients by comparing with dynamic gadolinium-enhanced MRI and histopathology. It has previously been demonstrated that the presence of glucose transporters in blood vessels surrounding high- and low-grade tumors is approximately inversely correlated with gadolinium-based contrast enhancement (24), which makes sense, because this reflects BBB functioning. However, gadolinium-based contrast enhancement does not have high specificity for distinguishing between high- and low-grade tumors (1, 2), and D-glucose enhancement could be more sensitive, a possibility that will have to be proven in future studies on more subjects.

DGE MRI (18) adds a new approach to a list of advanced agent-based dynamic MRI methods, including DCE (25) and DSC (26) MRI, as well as the recently emerging hyperpolarized $^{13}C$ approaches (27, 28), with substrates such as glucose (29) and pyruvate (30, 31). Each of these has particular advantages and disadvantages, and in many ways the methods are complementary and could be used in simultaneous or consecutive scans. Although not yet standard, DSC is becoming more routine in hospital settings and has the benefit of high MRI signal-to-noise ratio. DCE MRI is less common and less sensitive overall, but it has good signal-to-noise ratio properties in tumors with BBB disruption. The DCE response curve in principle contains information regarding tumor blood flow and BBB permeability, as well as intravascular volume and extravascular extracellular space (EES) in tumors. Compartmental modeling approaches to extract these parameters are becoming increasingly available. DSC approaches in principle provide blood volume and blood flow, but this is more difficult in tumors because of leakage of the contrast agent into the EES. Such problems can be reduced by using correction algorithms or by giving a pre-dose of contrast agent (32).

A major advantage of hyperpolarized $^{13}C$ MRI is that specific metabolic products can be detected together with the rate of their production (27, 28), which may provide crucial information regarding tumor malignancy, or to distinguish tumor progression from response to treatment (30, 31). Disadvantages include the need for an expensive hyperpolarizer and nonstandard (heteronuclear) radiofrequency coils as well as a limited acquisition window resulting from signal depolarization at the $T_1$ time scale. However, the availability of unique and relevant clinical information may make such investments worthwhile.

The DGE dynamic response curve (18) for glucose uptake contains information related to glucose delivery (perfusion and blood volume), transport into the tissue (BBB permeability and cell membrane transport), and metabolism. Because an AIF is also available, modeling approaches such as available for DCE should be a suitable first approach for obtaining information regarding intravascular volume, EES volume, and BBB permeability, but the theory will have to be adjusted to correct for signal disappearance resulting from cell transport and glucose metabolism. When using the initial part of the DGE curve before BBB transport, it may be possible to determine cerebral blood volume (CBV) and flow (CBF) in analogy to DSC, but it may be necessary to increase the speed of infusion, which is currently 1 min for 50 mL (ie, just under 1 mL/s). A combination of DCE, DSC, and DGE measurements may increase the accuracy of determining these different perfusion-related and metabolic parameters by analyzing the data in a multivariate manner. Such developments are expected in the future.

The current acquisition was performed at 7 T, and for DGE to become relevant clinically it would at least have to be possible at 3 T (and preferably at 1.5 T). The main obstacle to overcome is the proximity of the frequency of the hydroxyl proton saturation (1.2 ppm) to the water resonance, which corresponds to offsets ($\Delta\nu$) of 360, 154, and 77 Hz at 7, 3, and 1.5 T, respectively. There will thus be more interference of direct water saturation at lower fields, reducing the sensitivity for detecting glucose changes. In addition, the slow exchange limit for separating out the OH resonance (exchange rate, $k < 2\pi\Delta\nu$) for selective excitation or saturation no longer applies stringently at lower fields. However, these disadvantages are an issue mainly when using conventional frequency-selective saturation approaches. A new type of acquisitions called on-resonance exchange transfer technologies (33, 34) are becoming available that do not require selective excitation and can detect rapidly exchanging protons.

The translation of new contrast agents to actual clinical application is known to be time-consuming and expensive. We foresee we can accomplish fast translation for D-glucose based on existing FDA approval of intravenous D-glucose for other indications (the glucose tolerance test used daily in clinics around the country), which allowed us to gain IRB approval for the current experiments. For general application in the clinic, it will be needed to request an additional indication for D-glucose from the FDA for its use as an imaging agent, which we are currently in the process of doing. An important technical advantage that will facilitate rapid translation to the clinic is that CEST methods use the proton nucleus and can thus be performed immediately on standard clinical scanners without requiring additional equipment.

## CONCLUSIONS

DGE imaging is feasible in humans. Using DGE-MRI, it was possible to detect water signal changes in the human brain induced by the infusion of D-glucose. The signal changes are due to glucose uptake in the vessels, the brain, and tumor tissue areas, and are related to the kinetics of delivery, transport and metabolism of D-glucose. A very interesting first finding is that different tumor areas showed varying times of enhancement, which suggests that the dynamic time curves may contain information about BBB permeability. These findings provide preliminary support for the potential use of D-glucose as an MRI contrast agent and the use of DGE for studying glucose uptake properties of tumors and the brain, which are related to glucose delivery (perfusion), transport into the tissue (BBB and cell permeability), and metabolism.

The current acquisition was on a rather thick slice (6 mm) with a $3 \times 3$ mm$^2$ in-plane resolution that was comparable to typical arterial spin labeling acquisitions but more coarse than current DCE and DSC MRI. The CEST technology (35–38) is in the early stages of development, and we expect rapid advances toward whole-brain acquisition optimized for fast-exchanging protons close to the water resonance, such as those from the hydroxyl groups in D-glucose.

## Supplemental Materials

Video: http://tiny.cc/tom-01-02-s001

## ACKNOWLEDGMENTS

This research was supported by National Institutes of Health grants EB019934, CA103175, EB018934, and K23-DK093583. We are grateful to Terri Brawner, Kathleen Kahl, Ivana Kusevic, Kristine Mauldin, Stacey Quinlan, Tara Smith, Pamela Melvin, Craig Jones, and Joe Gillen for their assistance with the experiments and for optimizing the scanning, infusion, and blood-draw procedures. We thank Akimosa Jeffrey-Kwanisai, Yavette Morton, Lindsey Blair, and Prakash Ambady for their help in recruiting the volunteers and patients.

## REFERENCES

1. McKnight TR, Lamborn KR, Love TD, Berger MS, Chang S, Dillon WP, Bollen A, Nelson SJ. Correlation of magnetic resonance spectroscopic and growth characteristics within grades II and III gliomas. J Neurosurg. 2007;106(4):660–666.
2. Scott JN, Brasher PM, Sevick RJ, Rewcastle NB, Forsyth PA. How often are nonenhancing supratentorial gliomas malignant? A population study. Neurology. 2002; 59(6):947–949.
3. Kumar AJ, Leeds NE, Fuller GN, Van Tassel P, Maor MH, Sawaya RE, Levin VA. Malignant gliomas: MR imaging spectrum of radiation therapy- and chemotherapy-induced necrosis of the brain after treatment. Radiology. 2000;217(2):377–384.
4. Mullins ME, Barest GD, Schaefer PW, Hochberg FH, Gonzalez RG, Lev MH. Radiation necrosis versus glioma recurrence: conventional MR imaging clues to diagnosis. AJNR Am J Neuroradiol. 2005;26(8):1967–1972.
5. Sugahara T, Korogi Y, Tomiguchi S, Shigematsu Y, Ikushima I, Kira T, Liang L, Ushio Y, Takahashi M. Posttherapeutic intraaxial brain tumor: the value of perfusion-sensitive contrast-enhanced MR imaging for differentiating tumor recurrence from nonneoplastic contrast-enhancing tissue. AJNR Am J Neuroradiol. 2000; 21(5):901–909.
6. Thomsen HS, Morcos SK, Almen T, Bellin MF, Bertolotto M, Bongartz G, Clement O, Leander P, Heinz-Peer G, Reimer P, Stacul F, van der Molen A, Webb JA. Nephrogenic systemic fibrosis and gadolinium-based contrast media: updated ESUR Contrast Medium Safety Committee guidelines. Eur Radiol. 2013;23(2): 307–318.
7. FDA. http://www.fda.gov/Safety/MedWatch/SafetyInformation/SafetyAlertsforHumanMedicalProducts/ucm456012.htm.
8. McDonald RJ, McDonald JS, Kallmes DF, Jentoft ME, Murray DL, Thielen KR, Williamson EE, Eckel LJ. Intracranial gadolinium deposition after contrast-enhanced MR imaging. Radiology. 2015;275(3):772–782.
9. Chan KW, McMahon MT, Kato Y, Liu G, Bulte JW, Bhujwalla ZM, Artemov D, van Zijl PC. Natural D-glucose as a biodegradable MRI contrast agent for detecting cancer. Magn Reson Med. 2012;68(6):1764–1773.
10. Nasrallah FA, Pages G, Kuchel PW, Golay X, Chuang KH. Imaging brain deoxyglucose uptake and metabolism by glucoCEST MRI. J Cereb Blood Flow Metab. 2013;33(8):1270–1278.
11. Rivlin M, Horev J, Tsarfaty I, Navon G. Molecular imaging of tumors and metastases using chemical exchange saturation transfer (CEST) MRI. Sci Rep. 2013;3: 3045.
12. Walker-Samuel S, Ramasawmy R, Torrealdea F, Rega M, Rajkumar V, Johnson SP, Richardson S, Goncalves M, Parkes HG, Arstad E, Thomas DL, Pedley RB, Lythgoe MF, Golay X. In vivo imaging of glucose uptake and metabolism in tumors. Nat Med. 2013;19(8):1067–1072.
13. Gore JC, Brown MS, Mizumoto CT, Armitage IM. Influence of glycogen on water proton relaxation times. Magn Reson Med. 1986;3(3):463–466.
14. Jin T, Mehrens H, Hendrich KS, Kim SG. Mapping brain glucose uptake with chemical exchange-sensitive spin-lock magnetic resonance imaging. J Cereb Blood Flow Metab. 2014;34(8):1402–1410.
15. Yadav NN, Xu J, Bar-Shir A, Qin Q, Chan KW, Grgac K, Li W, McMahon MT, van Zijl PC. Natural D-glucose as a biodegradable MRI relaxation agent. Magn Reson Med. 2014;72(3):823–828.
16. Zu Z, Spear J, Li H, Xu J, Gore JC. Measurement of regional cerebral glucose uptake by magnetic resonance spin-lock imaging. Magn Reson Imaging. 2014; 32(9):1078–1084.
17. Rivlin M, Tsarfaty I, Navon G. Functional molecular imaging of tumors by chemical exchange saturation transfer MRI of 3-O-Methyl-D-glucose. Magn Reson Med. 2014;72(5):1375–1380.
18. Xu X, Chan KW, Knutsson L, Artemov D, Xu J, Liu G, Kato Y, Lal B, Laterra J, McMahon MT, van Zijl PC. Dynamic glucose enhanced (DGE) MRI for combined imaging of blood-brain barrier break down and increased blood volume in brain cancer. Magn Reson Med. 2015;74(6):1556–1563.
19. Lozner EL, Winkler AW, Taylor FH, Peters JP. The intravenous glucose tolerance test. J Clin Invest. 1941;20(5):507–515.
20. Diabetes Care. Standards of medical care in diabetes. http://care.diabetesjournals.org/content/suppl/2014/12/23/38.Supplement_1.DC1/January_Supplement_Combined_Final.6-99.pdf.
21. van Zijl PC, Jones CK, Ren J, Malloy CR, Sherry AD. MRI detection of glycogen in vivo by using chemical exchange saturation transfer imaging (glycoCEST). Proc Natl Acad Sci USA. 2007;104(11):4359–4364.
22. Zhou J, van Zijl P. Chemical exchange saturation transfer imaging and spectroscopy. Prog NMR Spectr. 2006;48(2-3):109–136.
23. Puri BK, Lewis HJ, Saeed N, Davey NJ. Volumetric change of the lateral ventricles in the human brain following glucose loading. Exp Physiol. 1999;84(1):223–226.
24. Guerin C, Laterra J, Hruban RH, Brem H, Drewes LR, Goldstein GW. The glucose transporter and blood-brain barrier of human brain tumors. Ann Neurol. 1990; 28(6):758–765.
25. Dujardin MI, Sourbron SP, Chaskis C, Verellen D, Stadnik T, de Mey J, Luypaert R. Quantification of cerebral tumour blood flow and permeability with T1-weighted dynamic contrast enhanced MRI: a feasibility study. J Neuroradiol. 2012;39(4):227–235.
26. Lupo JM, Cha S, Chang SM, Nelson SJ. Dynamic susceptibility-weighted perfusion imaging of high-grade gliomas: characterization of spatial heterogeneity. AJNR Am J Neuroradiol. 2005;26(6):1446–1454.
27. Brindle KM, Bohndiek SE, Gallagher FA, Kettunen MI. Tumor imaging using hyperpolarized 13C magnetic resonance spectroscopy. Magn Reson Med. 2011; 66(2):505–519.
28. Park I, Larson PE, Zierhut ML, Hu S, Bok R, Ozawa T, Kurhanewicz J, Vigneron DB, Vandenberg SR, James CD, Nelson SJ. Hyperpolarized 13C magnetic resonance metabolic imaging: application to brain tumors. Neuro Oncol. 2010; 12(2):133–144.
29. Rodrigues TB, Serrao EM, Kennedy BW, Hu DE, Kettunen MI, Brindle KM. Magnetic resonance imaging of tumor glycolysis using hyperpolarized 13C-labeled glucose. Nat Med. 2014;20(1):93–97.
30. Day SE, Kettunen MI, Cherukuri MK, Mitchell JB, Lizak MJ, Morris HD, Matsumoto S, Koretsky AP, Brindle KM. Detecting response of rat C6 glioma tumors to radiotherapy using hyperpolarized [1-13C]pyruvate and 13C magnetic resonance spectroscopic imaging. Magn Reson Med. 2011;65(2):557–563.
31. Park I, Bok R, Ozawa T, Phillips JJ, James CD, Vigneron DB, Ronen SM, Nelson SJ. Detection of early response to temozolomide treatment in brain tumors using hyperpolarized 13C MR metabolic imaging. J Magn Reson Imaging. 2011; 33(6):1284–1290.
32. Knutsson L, Stahlberg F, Wirestam R. Absolute quantification of perfusion using dynamic susceptibility contrast MRI: pitfalls and possibilities. MAGMA. 2010; 23(1):1–21.
33. Vinogradov E, Zhang S, Lubag A, Balschi JA, Sherry AD, Lenkinski RE. On-resonance low B1 pulses for imaging of the effects of PARACEST agents. J Magn Reson. 2005;176(1):54–63.
34. Yadav NN, Jones CK, Xu J, Bar-Shir A, Gilad AA, McMahon MT, van Zijl PC. Detection of rapidly exchanging compounds using on-resonance frequency-labeled exchange (FLEX) transfer. Magn Reson Med. 2012;68(4):1048–1055.
35. Kogan F, Hariharan H, Reddy R. Chemical exchange saturation transfer (CEST) imaging: description of technique and potential clinical applications. Curr Radiol Rep. 2013;1(2):102–114.
36. van Zijl PC, Yadav NN. Chemical exchange saturation transfer (CEST): what is in a name and what isn't? Magn Reson Med. 2011;65(4):927–948.
37. Vinogradov E, Sherry AD, Lenkinski RE. CEST: from basic principles to applications, challenges and opportunities. J Magn Reson. 2013;229:155–172.
38. Ward KM, Aletras AH, Balaban RS. A new class of contrast agents for MRI based on proton chemical exchange dependent saturation transfer (CEST). J Magn Reson. 2000;143(1):79–87.